Solvatomorphs of dimeric transition metal complexes based on the V_4O_{12} cyclic anion as building block: Crystalline packing and magnetic properties

V. Paredes-García [a,c], S. Gaune [a], M. Saldías [b], M.T. Garland [b,c], R. Baggio [d], A. Vega [e], M. Salah El Fallah [f], A. Escuer [f], E. Le Fur [g], D. Venegas-Yazigi [c,h], E. Spodine [c,i,*]

[a] Departamento de Química, Universidad Tecnológica Metropolitana, Chile
[b] Facultad de Ciencias Físicas y Matemáticas, Universidad de Chile, Chile
[c] CIMAT, Universidad de Chile, Chile
[d] Departamento de Física, Comisión Nacional de Energía Atómica, Argentina
[e] Facultad de Ecología y Recursos Naturales, Universidad Nacional Andrés Bello, Chile
[f] Departamento de Química Inorgánica, Universitat de Barcelona, Barcelona, Spain
[g] Sciences Chimiques, UMR CNRS 6226, Rennes, France
[h] Facultad de Química y Biología, Universidad de Santiago de Chile, Chile
[i] Facultad de Ciencias Químicas y Farmacéuticas, Universidad de Chile, Chile

A B S T R A C T

Dinuclear $[\{M(phen)_2\}_2V_4O_{12}] \cdot C_6H_{12}O \cdot H_2O$ (M = Co^{II} **1**, Mn^{II} **2**, Ni^{II} **3** and Cu^{II} **4**) and $[\{Cu(phen)_2\}_2V_4O_{12}] \cdot 3.5H_2O$ **5** has been prepared by biphasic and hydrothermal syntheses, respectively. All five structures exhibit the $\{V_4O_{12}\}^{4-}$ cluster in a chair-like configuration, covalently bonded to two $[M(phen)_2]^{2+}$ fragments, producing a super-exchange magnetic phenomenon. The magnetic study of complexes **1**–**5** shows that they are very weak antiferromagnetically coupled systems, with J values of −0.14, **2**; −0.64, **3** and −0.23, **4** cm^{-1}. Complexes **1** to **3** correspond to isostructural compounds in which the cyclovanadate group acts as a bidentate bridged ligand. In the copper complexes (**4** and **5**) the $\{V_4O_{12}\}^{4-}$ anion presents the novel monodentate bridging mode, and therefore a more significant distortion from the chair-like configuration. The mentioned complexes, together with that reported in the literature, permit to conclude that it is quite common for a single molecular species to exist in more than one crystalline arrangement. A detailed analysis of the structures of **1**–**4** shows that the crystal symmetry cannot be strictly centrosymmetric, due to the presence of the cyclohexanol molecule with a single –OH group in the lattice.

Keywords:
Cyclic vanadate bridge
Transition metal complexes
Crystalline packing
Magnetic properties

1. Introduction

The chemistry of polyoxovanadate compounds ranges from extended systems such as infinite chains, layered and three dimensional structures to discrete molecular units [1–4]. Among the latter the discrete clusters $V_4O_{12}^{4-}$, $V_6O_{12}^{8-}$, $V_8O_{23}^{4-}$ and $V_{10}O_{29}^{8-}$ in bimetallic compounds can be mentioned [5–12]. At present, the hydrothermal syntheses of hybrid organo-inorganic compounds based on vanadium oxides are of great interest, since by incorporating organic and inorganic components into a single structure, the topological diversity of the obtained materials can be first multiplied and then tailored. These hybrid materials present potential applications in catalysis, electron conductivity, magnetism and photochemistry. If micro-porous solids are obtained, they can also be tested for molecular absorption, exchange and heterogeneous catalysis [13–17].

Owing to the ability of vanadium to adopt a variety of coordination geometries in various oxidation states, the influences of the second metal ions as well as that of the organic ligands on the structure can be significant. Therefore, novel structural types can be discovered by modifying these parameters, together with the synthetic conditions [12].

The VO_4 group is an important building block of many polynuclear species, mainly obtained under hydrothermal conditions. This is due to its interlinkage capacity, by way of which the tetrahedra can interconnect to each other into a large diversity of oligomeric species. A well-known example is the $\{V_4O_{12}\}^{4-}$ ring obtained from four tetrahedral units sharing one corner each, and characterized by a closed internal V_4O_4 cycle with eight external oxygen atoms. The latter can behave as active sites prone to coordination, as proved by the many transition metal mixed complexes, where the ring takes part as a ligand [18].

* Corresponding author. Tel.: +56 2 978 2862; fax: +56 2 978 2868.
E-mail address: espodine@uchile.cl (E. Spodine).

The use of different solvent media to obtain polymetallic compounds can lead to similar molecular structures, but different solvatomorphs which crystallize in different symmetry groups. This fact may affect the bulk magnetic properties which are strongly determined not only by molecular distortions, but also by crystal packing.

In this work we inform the hydrothermal syntheses, crystal structures and magnetic properties of five homo-binuclear complexes containing the $\{V_4O_{12}\}^{4-}$ cluster $[\{Co(phen)_2\}_2V_4O_{12}]\cdot C_6H_{12}O\cdot H_2O$ **1**, $[\{Mn(phen)_2\}_2V_4O_{12}]\cdot C_6H_{12}O\cdot H_2O$ **2**, $[\{Ni(phen)_2\}_2V_4O_{12}]\cdot C_6H_{12}O\cdot H_2O$ **3**, $[\{Cu(phen)_2\}_2V_4O_{12}]\cdot C_6H_{12}O\cdot H_2O$ **4** and $[\{Cu(phen)_2\}_2V_4O_{12}]\cdot 3.5H_2O$ **5**. The five structures exhibit the $\{V_4O_{12}\}^{4-}$ cluster in a chair-like configuration, covalently bonded to two $[M(phen)_2]^{2+}$ fragments. Complexes **1** to **3** correspond to isostructural compounds in which the cyclovanadate group acts as a bidentate bridged ligand. In the copper complexes (**4** and **5**) the $\{V_4O_{12}\}^{4-}$ anion acts as a monodentate bridging ligand, presenting furthermore a more significant distortion from the chair-like configuration.

2. Experimental

All reagents were purchased from Merck or Aldrich, and used without further purification.

2.1. $[M_2(phen)_4V_4O_{12}]\cdot C_6H_{11}OH\cdot H_2O$ (**1**–**4**)

The biphasic hydro/solvothermal reactions to obtain complexes **1** to **4** were carried out in a 23 mL Teflon-lined stainless steel autoclave at 120 °C for 5 h under autogenous pressure. After slow cooling to room temperature the obtained solid was filtered and dried at 40 °C.

The cobalt, manganese, nickel and copper chlorides and sodium phosphate were used as 1 M and 2 M aqueous solutions, respectively. A 1 M cyclohexanol solution of 1,10-phenanthroline (phen) was used, and the V_2O_5 was added as a solid phase. The final molar ratio for the metal salt, sodium phosphate, phen and V_2O_5 was 1:5:1:2, respectively.

X-ray diffraction quality single crystals were directly separated from the bulk, as violet crystals for $[Co_2(phen)_4V_4O_{12}]\cdot C_6H_{11}OH\cdot H_2O$, **1**, red for $[Mn_2(phen)_4V_4O_{12}]\cdot C_6H_{11}OH\cdot H_2O$, **2**, green for $[Ni_2(phen)_4V_4O_{12}]\cdot C_6H_{11}OH\cdot H_2O$, **3** and greenish-blue for $[Cu_2(phen)_4V_4O_{12}]\cdot C_6H_{11}OH\cdot H_2O$, **4**.

2.2. $[Cu_2(phen)_4V_4O_{12}]\cdot 3.5H_2O$ (**5**)

Compound **5** was obtained by hydrothermal synthesis using a suspension of $Cu(NO_3)_2\cdot H_2O$, Na_3PO_4, phen, V_2O_4 in water, in a molar ratio of 2:5:4:1:660. The mixture was heated in a 23 mL Teflon-lined stainless steel autoclave at 120 °C for 72 h, followed by slow cooling to room temperature. The resulting product was filtered off and dried at 40 °C. Well formed greenish-blue crystals were isolated from the bulk material.

The IR spectra exhibit strong intensity absorption bands in the range of 1600–1200 cm^{-1} attributed to the 1,10-phenanthroline ligand. The bands at 950–900 cm^{-1} are assigned to ν (V=O), and at 750 and 640 cm^{-1} assigned to V–O–V stretching.

2.3. Single-crystal X-ray diffraction

The crystal structures of **1** to **5** at room temperature were determined by single crystal X-ray diffraction. Besides, the structure of **2** was also determined at 120 K, showing no major changes in relation to the room temperature determination. The crystal structure of **2** was also measured at liquid helium temperature (30 K). The structure at low temperature was recorded on a Bruker Smart-1K CCD diffractometer, equipped with an Oxford Cryosystem Helix He open flow cryostat.

Each crystal was glued with epoxy resin on the tip of a capillary glass, and then mounted at room temperature on a SMART-APEX Bruker diffraction system [19]. A complete data set was measured for each compound, using 10 s by frame and 0.3° rotation between them. Reciprocal space exploration using RLATT [20] showed good crystal quality in each case. Data reduction was done with SAINT-PLUS [21], while the structure solution, completion and refinement were conducted with SHELXTL [22]. Empirical absorption corrections were applied using SADABS [23]. Tabulated *R*-values for the final cycle of the refinements based on F_0^2, together with additional data collection and refinement details, are given in Tables 1 and 2. In all cases the hydrogen atoms were included at calculated positions and constraintly refined. It was not possible to find the hydrogen atoms of the water solvate molecules.

During the last stages of refinement of compounds **1**–**4** some configurational disorder was noted in the location of the cyclohexanol –OH group. It was modelled using two equally occupied positions adding one in a 1,4 correlation within the C_6 ring, as imposed by the crystallographic inversion centre. For the data of **2**, obtained at helium temperature, there is also some disorder on the cyclohexanol ring which was modelled with two partially occupied positions.

The $\{V_4O_{12}\}^{4-}$ ring in compound **5** presented some noticeable disorder during the last stages of refinement. It was modelled using two positions with fractional occupancies, which were refined and then held constant at 0.53/0.47, respectively. Three and a half solvating water molecules were found to partially occupy four different positions.

2.4. Magnetic susceptibility

Magnetic susceptibility measurements for **1**–**4** were carried out on polycrystalline samples, at the Servei de Magnetoquímica of the Universitat de Barcelona, with a Quantum Design SQUID MPMS-XL susceptometer apparatus working in the range 2–300 K under magnetic fields of approximately 0.1 T. The magnetization curves were recorded at 2 K at fields ranging from 0 to 5 T. Diamagnetic corrections were estimated from Pascal constants.

3. Results and discussion

3.1. Structural description

The first three $[M_2(phen)_4V_4O_{12}]\cdot C_6H_{11}OH\cdot H_2O$ complexes of the series are isostructural, where M = Co^{II}, **1**, Mn^{II}, **2** and Ni^{II}, **3**. All the description for complex **2** is based on the room temperature data. The low temperature structures for this same compound show almost no differences compared with the room temperature one.

The compounds present an M^{II} centre with a distorted octahedral geometry. It coordinates to four nitrogen atoms from two diimine ligands and two terminal oxygen atoms of adjacent vanadium sites of the ring. These atoms form an isolated neutral hexanuclear heterometallic cluster, which is built up from a central eight-membered $\{V_4O_{12}\}^{4-}$ ring, and two terminal $M(phen)_2$ moieties. The discrete $\{V_4O_{12}\}^{4-}$ cluster is constructed from four VO_4 tetrahedra connected through the oxo group (O_b) in such a way as to define an alternating V–O octa-membered ring, with two terminal oxygen atoms (O_t) on each vanadium atom. Selected bond distances and angles are listed in Table 3, while Fig. 1 shows a displacement ellipsoid diagram for structure **1**, as representative of the isostructural group **1** to **3**.

Table 1
Crystal data and structure refinement for $[M_2(phen)_4V_4O_{12}] \cdot C_6H_{11}\,OH \cdot H_2O$, **1**–**3**

	M = Co, **1**	M = Mn, **2**	M = Ni, **3**
FW/uma	1350.59	1342.61	1350.15
Crystal system	Triclinic	Triclinic	Triclinic
Space group	$P\bar{1}$	$P\bar{1}$	$P\bar{1}$
a (Å)	10.6488(15)	10.6860(14)	10.5882(18)
b (Å)	10.6658(15)	10.6781(14)	10.6683(18)
c (Å)	13.0837(18)	13.0960(18)	13.067(2)
α (°)	75.678(2)	76.732(2)	75.320(3)
β (°)	89.060(2)	89.394(2)	88.914(3)
γ (°)	68.608(2)	69.180(2)	68.434(3)
V (Å^3)	1336.1(3)	1355.3(3)	1323.4(4)
Z (Z')	1 (0.5)	1 (0.5)	1 (0.5)
δ (g cm^{-3})	1.678	1.645	1.694
μ (mm^{-1})	1.353	1.188	1.451
$F(000)$	682	678	684
θ Range (°)	2.06–27.94	1.60–28.08	2.08–28.09
hkl Range	$-13 \leqslant h \leqslant 14$ $-13 \leqslant k \leqslant 13$ $-17 \leqslant l \leqslant 16$	$-13 \leqslant h \leqslant 13$ $-14 \leqslant k \leqslant 14$ $-17 \leqslant l \leqslant 17$	$-13 \leqslant h \leqslant 13$ $-13 \leqslant k \leqslant 13$ $-16 \leqslant l \leqslant 17$
N_{tot}, N_{uniq} (R_{int}), N_{obs}	11308, 5791 (0.0246), 4478	11538, 5875 (0.0712), 3230	11328, 5781 (0.0443), 3649
Refinement parameters	379	379	379
Goodness-of-fit (GOF)	0.974	0.804	0.957
R_1, wR_2 (obs)	0.0523, 0.1374	0.0644, 0.1408	0.0624, 0.1326
R_1, wR_2 (all)	0.0690, 0.1493	0.1261, 0.1763	0.1072, 0.1503
Maximum and minimum $\Delta\rho$	0.752 and −0.318	0.678 and −0.356	0.618 and −0.355

Table 2
Crystal data and structure refinement for $[Cu_2(phen)_4V_4O_{12}] \cdot C_6H_{11}OH \cdot H_2O$ **4** and $[Cu_2(phen)_4V_4O_{12}] \cdot 3.5H_2O$, **5**

	M = Cu, **4**	M = Cu, **5**
FW/uma	1359.81	1298.74
Crystal system	Triclinic	Monoclinic
Space group	$P\bar{1}$	$P2_1/n$
a (Å)	14.2042(14)	14.7211(14)
b (Å)	14.5651(14)	13.5544(13)
c (Å)	16.0649(15)	25.495(2)
α (°)	107.757(2)	90
β (°)	100.906(2)	106.040(2)
γ (°)	115.966(2)	90
V (Å^3)	2635.8(4)	4889.1(8)
Z (Z')	2 (1)	4
δ (g cm^{-3})	1.713	1.766
μ (mm^{-1})	1.549	1.668
$F(000)$	1372	2600
θ Range (°)	1.44–28.07	1.66–25.19
hkl Range	$-17 \leqslant h \leqslant 17$ $-19 \leqslant k \leqslant 19$ $-20 \leqslant l \leqslant 20$	$-17 \leqslant h \leqslant 17$ $-16 \leqslant k \leqslant 16$ $-30 \leqslant l \leqslant 30$
N_{tot}, N_{uniq} (R_{int}), N_{obs}	22501, 11478 (0.0428), 7486	30358, 8763 (0.1675), 4788
Refinement parameters	748	757
Goodness-of-fit (GOF)	1.018	0.994
R_1, wR_2 (obs)	0.0628, 0.1297	0.0811, 0.1868
R_1, wR_2 (all)	0.1031, 0.1490	0.1525, 0.1868
Maximum and minimum $\Delta\rho$	0.806 and −0.386	1.088 and −1.034

Table 3
Selected bond distances (Å) and angles (°) for **1**–**3**

	M = Co, **1**	M = Mn, **2**	M = Ni, **3**
Co1–O1	2.076(2)	2.102(4)	2.077(3)
Co1–O2	2.025(2)	2.085(4)	2.027(3)
Co1–N1	2.137(3)	2.266(5)	2.089(4)
Co1–N2	2.168(3)	2.292(5)	2.102(4)
Co1–N3	2.140(3)	2.258(5)	2.081(4)
Co1–N4	2.157(3)	2.303(5)	2.089(4)
V1–O1	1.671(2)	1.662(4)	1.663(3)
V1–O3a	1.782(3)	1.774(4)	1.782(4)
V1–O5	1.783(3)	1.782(4)	1.784(4)
V1–O6	1.612(2)	1.609(4)	1.610(3)
V2–O2	1.656(2)	1.650(4)	1.648(3)
V2–O3	1.789(3)	1.787(4)	1.793(3)
V2–O4	1.606(3)	1.595(4)	1.597(4)
V2–O5	1.800(2)	1.795(4)	1.804(3)
O2–Co1–O1	91.65(10)	93.66(15)	90.31(13)
O2–Co1–N1	95.55(11)	100.80(18)	92.90(15)
O1–Co1–N1	93.78(11)	91.52(16)	93.23(14)
O2–Co1–N3	93.00(11)	91.99(18)	93.12(15)
O1–Co1–N3	95.70(10)	102.56(16)	94.39(14)
N1–Co1–N3	167.04(11)	160.37(16)	170.26(15)
O2–Co1–N4	169.94(11)	164.65(18)	172.24(15)
O1–Co1–N4	88.47(11)	90.93(16)	88.22(14)
N1–Co1–N4	94.48(11)	93.71(17)	94.80(15)
N3–Co1–N4	76.99(11)	72.71(18)	79.40(16)
O2–Co1–N2	86.98(10)	87.60(16)	87.14(14)
O1–Co1–N2	170.70(10)	163.98(17)	172.06(14)
N1–Co1–N2	77.21(11)	72.58(17)	79.40(16)
N3–Co1–N2	93.57(10)	93.35(16)	93.25(15)
N4–Co1–N2	94.49(11)	92.01(17)	95.29(15)
O6–V1–O1	109.70(13)	109.8(2)	109.43(17)
O6–V1–O3a	110.00(14)	110.2(2)	109.95(19)
O1–V1–O3a	109.35(12)	109.7(2)	109.25(17)
O6–V1–O5	109.11(14)	108.9(2)	108.86(19)
O1–V1–O5	108.80(12)	108.34(19)	109.55(17)
O3–V1–O5a	109.87(13)	110.0(2)	109.80(17)
O4–V2–O2	108.86(16)	109.2(3)	109.2(2)
O4-V2–O3	109.74(14)	108.8(2)	109.66(19)
O2–V2–O3	110.19(13)	110.1(2)	110.36(16)
O4–V2–O5	108.62(13)	108.6(2)	108.19(18)
O2–V2–O5	107.51(12)	108.2(2)	107.46(17)
O3–V2–O5	111.83(13)	111.88(19)	111.88(17)
V1–O3–V2a	142.39(17)	144.1(3)	141.5(2)
V1–O5–V2	126.36(14)	129.5(2)	124.80(19)

a: $-x+1$, $-y+1$, $-z$.

The V–O distances in compounds **1**–**3** (1.595(4) to 1.803(3) Å) are all normal for the vanadate anion, and compare well with those observed for other compounds that contain a $\{V_4O_{12}\}^{4-}$ ring [24]. The V–O_t bond distances are all short, ranging from 1.595(4) to 1.612(2) Å, while the V–O_b bond lengths present short exocyclic V1–O1 distances (1.657(2) for **1**, 1.650(4) for **2** and 1.647(3) Å for **3**), and the short exocyclic V2–O5 distances (1.612(2) for **1**, 1.609(4) for **2** and 1.609(3) Å for **3**); while the rest of the endocyclic V–O_b bond lengths are in the order of 1.8 Å.

All the V–O–V bond angles are within the range of 108.2(2) and 111.9(2)°, close to the value of the tetrahedral angle. The V–O–V angles alternate within the ring, compound **1** presenting the largest angle and compound **3** the smallest (V2a–O3–V1: 144.1(3) for **1**, 142.34(17) for **2** and 141.6(2)° for **3**; V2–O4–V1: 129.5(2) for **1**, 126.35(14) for **2** and 124.77(18)° for **3**). The four vanadium atoms in the ring are strictly coplanar, because of the crystal inversion centre.

The V–O–M angle in these compounds presents two values: approximately 134° for the V2–O6–M, and the more obtuse angle associated with the short V–O_b distance (V1–O1–M: 137.1(2) for **1**, 141.19(14) for **2** and 142.37(18)° for **3**). If the oxygen atoms of alternate vanadium sites are used to chelate the metal centres, an even more open V–O–M angle is generated in the structure [5]. This endows the cluster with a twisted chair-like configuration.

The copper(II) binuclear compounds $[Cu_2(phen)_4V_4O_{12}]$ **4** and **5** present the same $\{V_4O_{12}\}^{4-}$ bridging ring as the **1**–**3** complexes (Fig. 2). However, the vanadium (V) cycle is bonded to the copper(II) atoms in a monodentate fashion.

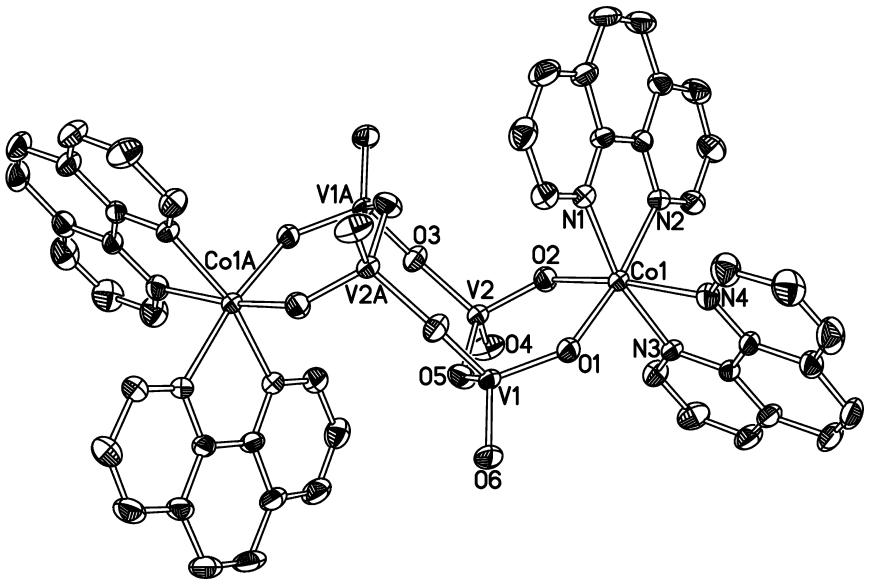

Fig. 1. Structure of the isostructural $[Co_2(phen)_4V_4O_{12}] \cdot C_6H_{11}OH \cdot H_2O$ complex (**1**).

Table 4
Selected bond distances (Å) and angles (°) for copper(II) complexes **4** and **5**

M = Cu, **4**

Molecule **A**		Molecule **B**	
Cu1A–O1A	1.894(3)	Cu1B–O1B	1.907(3)
Cu1A–N1A	2.163(4)	Cu1B–N1B	2.130(4)
Cu1A–N2A	2.014(4)	Cu1B–N2B	1.971(4)
Cu1A–N3A	2.080(4)	Cu1B–N3B	2.113(4)
Cu1A–N4A	1.987(4)	Cu1B–N4B	1.973(4)
V1A–O1A	1.667(3)	V1B–O1B	1.666(3)
V1A–O2A	1.621(4)	V1B–O2B	1.604(3)
V1A–O3A	1.756(3)	V1B–O3B	1.786(3)
V1A–O4A	1.747(3)	V1B–O4B	1.777(3)
V2A–O3Aa	1.799(3)	V2B–O3Bb	1.801(3)
V2A–O4A	1.800(3)	V2B–O4B	1.796(3)
V2A–O5A	1.610(4)	V2B–O5B	1.623(3)
V2A–O6A	1.614(4)	V2B–O6B	1.617(3)
O1A–Cu1A–N1A	119.30(15)	O1B–Cu1B–N1B	134.23(16)
O1A–Cu1A–N2A	95.82(15)	O1B–Cu1B–N2B	97.29(15)
O1A–Cu1A–N3A	147.68(16)	O1B–Cu1B–N3B	126.51(15)
O1A–Cu1A–N4A	92.74(15)	O1B–Cu1B–N4B	91.79(15)
O1A–V1A–O3A	110.71(17)	O1B–V1B–O3B	112.46(17)
O1A–V1A–O4A	108.6(2)	O1B–V1B–O4B	108.16(18)
O2A–V1A–O1A	109.02(19)	O2B–V1B–O1B	109.13(18)
O2A–V1A–O4A	108.3(2)	O2B–V1B–O4B	108.78(18)
V1A–O3A–V2Aa	154.2(2)	V1B–O3B–V2Bb	135.2(2)
V1A–O4A–V2A	145.6(2)	V1B–O4B–V2B	135.8(2)

M = Cu, **5**

Cu1–O1	1.914(6)	Cu2–N8	1.975(6)
Cu2–O9	1.941(6)	V1–O1	1.634(6)
Cu1–N1	1.983(6)	V1–O4	1.751(5)
Cu1–N2	2.193(7)	V2–O4	1.747(5)
Cu1–N3	1.985(6)	V3–O8	1.631(7)
Cu1–N4	2.058(6)	V3–O9	1.640(6)
Cu2–N5	1.982(6)	V3–O10	1.719(5)
Cu2–N6	2.190(7)	V4–O10	1.783(6)
Cu2–N7	2.054(7)	V4–O12	1.603(6)
O1–Cu1–N1	94.1(2)	O1–V1–O4	110.7(3)
O1–Cu1–N2	97.7(3)	O8–V3–O9	109.9(3)
O1–Cu1–N3	158.9(3)	O8–V3–O10	111.6(3)
O1–Cu1–N4	91.0(3)	O9–V3–O10	107.4(3)
O9–Cu2–N5	92.4(3)	O12–V4–O10	111.2(3)
O9–Cu2–N6	101.1(2)	V2–O4–V1	150.4(4)
O9–Cu2–N7	150.6(3)	V3–O10–V4	143.6(4)
O9–Cu2–N8	95.0(3)		

a:1 − *x*,1 − *y*,1 − *z*; *b*: − *x*,1 − *y*, − *z*.

Compound **4**, obtained by the biphasic water/cyclohexanol synthesis, crystallizes with two different complex molecules in the asymmetric unit (named **A** and **B)** (see Table 4). While **A** presents V1A–O1A–Cu1A angle of 136.9(2)°, **B** has a more obtuse angle of 163.3(2)°. The V–O–V angles corresponding to the ring are 154.2(2) and 145.6(2)° for **A**, and 135.2(2) and 135.8(2)° for **B**.

The endocyclic V–O bond distances are in the range of 1.747(3) to 1.800(3) Å for **A**, and 1.777(3) to 1.80(3) Å for **B**. The exocyclic V–O bond distances, corresponding to the oxygen atom coordinated to copper (II), are 1.667(3) Å for **A** and 1.666(3) Å for **B**.

The copper (II) centres of **A** and **B** are pentacoordinated. However, they present different distorted coordination environments: both copper (II) centres in **A** are best described as a distorted square base pyramid ($\tau = 0.39$), while those of **B** correspond to a distorted trigonal bipyramid ($\tau = 0.61$).

Compound **5** was obtained by hydrothermal synthesis from a V^{IV} precursor, V_2O_4. This shows the possibility of oxidizing the vanadium precursor to V^V, by using $Cu(NO_3)_2$ as the copper(II) source [25]. It is important to point out that previous reports of hydrothermal syntheses indicate that reduction of V^V can be observed in the presence of diimine ligands and higher temperatures [26]. This compound also presents the bridging $\{V_4O_{12}\}^{4-}$ unit, connected in a monodentate fashion to the $[M(phen)_2]^{2+}$ moieties. The molecule has two similar but not equivalent copper(II) centres, both best described to have a distorted square pyramidal geometry ($\tau = 0.24$ for Cu1, and 0.34 for Cu2).

Except for the water molecule in **4**, all the solvates are disordered; the hydration water molecules in **1**–**3** lie on a general position with partial occupancy of 0.5, while the cyclohexanol hydroxyl group is disordered over two half occupied positions in a 1,4 correlation in the aliphatic C_6 ring, as imposed by the crystallographic symmetry centre.

In all the studied complexes, the intermolecular interaction scheme shows interconnecting moieties via hydrogen bonding. Unfortunately, the water hydrogen atoms could not be found so as to make a clearer picture of the role of H-bonding in the packing mode. As usual in compounds where planar rings with a π-system are present, the availability of aromatic rings gives rise to a number of π–π and C–H···π interactions in the packing. The more relevant are summarized in Table 5, in terms of plane to plane distance (ppd) and centroid to centroid distance (ccd).

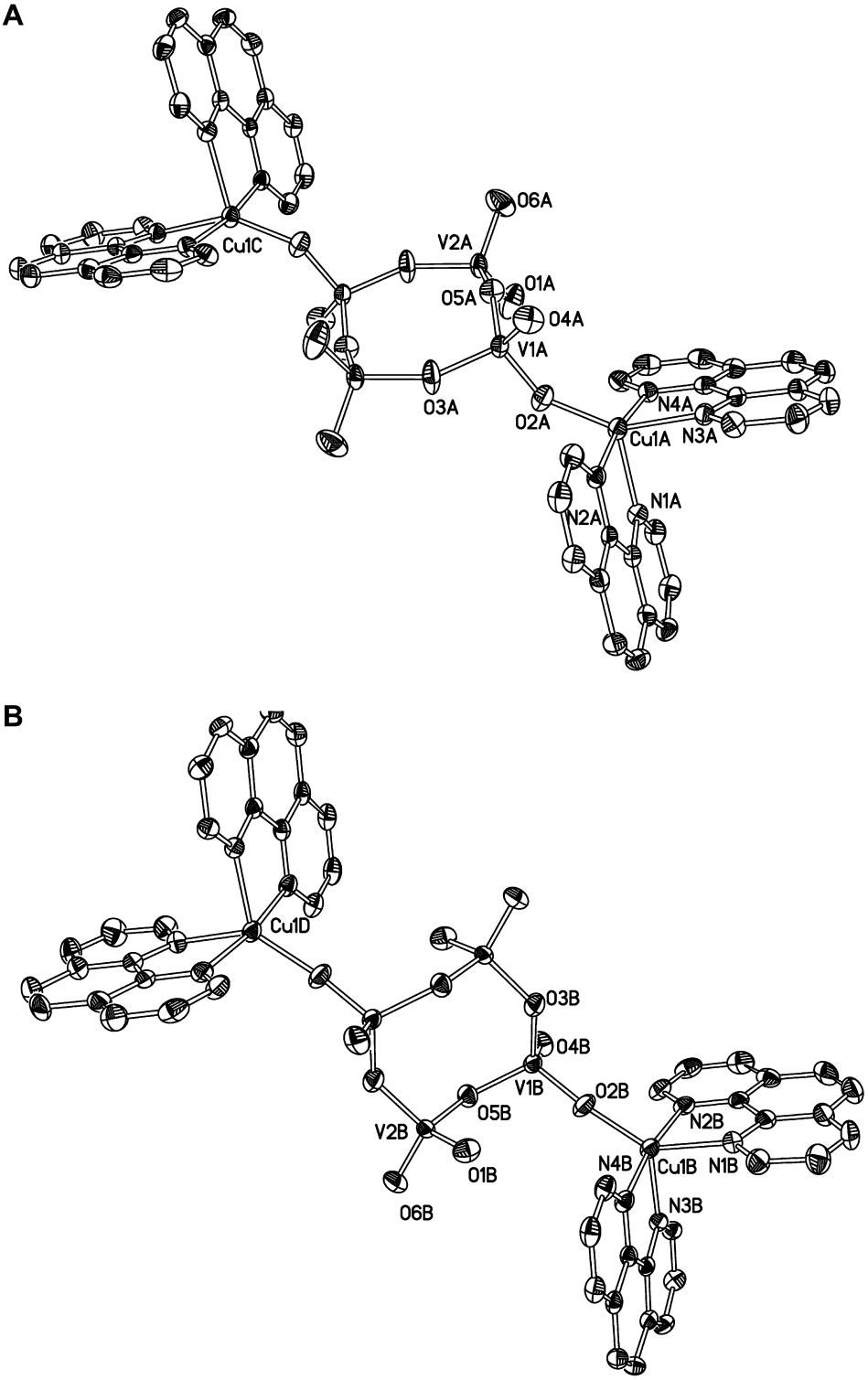

Fig. 2. Structure of the $[Cu_2(phen)_4V_4O_{12}] \cdot C_6H_{11}OH \cdot H_2O$ complex (**4**). Labels A and B represent the two different half molecules, while C and D represent the $1 - x$,$1 - y$, $1 - z$ and $-x$, $-y + 1$, $-z$ symmetry equivalents, respectively. Hydrogen atoms were omitted for clarity.

The dimeric molecular units of complex **5** define a sort of non-covalent chain along the ***a***-cell axis. The phenanthroline ligand (N3–N4) is stacked at 3.45(1) Å with the ring (N7–N8) coordinated to that of the nearest neighbour cupric centre ($x - 1$, y, z). These linear chains are packed in the crystal in a zipper-like arrangement of stacked phenanthroline groups. The aromatic groups which are perpendicular to each ***a***-chain interact with phenanthroline groups from a vicinal chain, as schematized in Fig. 3. The N1–N2 phenanthroline groups are in this way stacked at 3.42(1) Å with its $1 - x$, $2 - y$, $-z$ equivalent group; while the N4–N5 ring lies at 3.40(2) Å from the $x - 1/2$, $3/2 - y$, $z - 1/2$ equivalent of the N1-N2 ring.

Table 5
π–π/C–H···π contacts for **1**–**5**

Structure		Cg/C–H···Cg	ccd (Å)	ipd (Å)
1		Cg2 Cg2#1	3.730	3.47(1)
		Cg2 Cg6#2	3.878	3.39(1)
		Cg6 Cg6#2	3.504	3.39(1)
		C20–H20 Cg8#3	2.67	2.64
2		Cg2 Cg2#1	3.707	3.46(1)
		Cg2 Cg5#1	3.945	3.44(1)
		Cg3 Cg6#2	3.818	3.43(1)
		Cg6 Cg6#2	3.529	3.42(1)
		C20–H20 Cg(5)#3	2.64	2.61
3		Cg2 Cg2#1	3.769	3.49(1)
		Cg2 Cg5#1	4.034	3.49(2)
		Cg3 Cg6#2	3.896	3.38(2)
		Cg6 Cg6#2	3.500	3.38(1)
		C20–H20 Cg5#3	2.65	8.27
4	Molecule **A**	Cg1 Cg2#4	3.684	3.41(1)
		Cg1 Cg5#4	3.678	3.43(3)
		Cg3 Cg4#5	3.722	3.43(1)
		Cg4 Cg6#5	3.751	3.45(2)
		Cg5 Cg5#4	3.746	3.47(1)
		Cg6 Cg6#5	3.689	3.46(1)
	Molecule **B**	Cg1 Cg2#6	4.010	3.41(2)
		Cg1 Cg5#6	3.741	3.51(1)
		Cg3 Cg6#7	3.818	3.40(3)
		Cg6 Cg6#7	3.482	3.41(1)
5		Cg7 Cg5#8	4.136	3.40(2)
		Cg8 Cg5#8	3.523	3.40(2)
		Cg2 Cg5#9	4.438	3.42(1)
		Cg5 Cg2#9	3.771	3.42(1)
		Cg3 Cg11#10	3.841	3.45(1)
		Cg4 Cg10#10	3.874	3.45(1)
		Cg6 Cg9#10	3.623	3.45(1)

Cg denotes the centroid of a six-membered ring, ccd denotes the centroid to centroid (or H to centroid) distance (Å), ipd is the (mean) plane to plane (or H to plane) distance (Å).
Symmetry codes: #1: 2 − *x*, −*y*, −*z*; #2: 1 − *x*, −*y*, 1 − *z*; #3: 2 − *x*, −*y*, 1 − *z*; #4: −*x*, 1 − *y*, 1 − *z*; #5: 1 − *x*, 2 − *y*, 1 − *z*; #6: −*x*, −*y*, −*z*; #7: 1 − *x*, 1 − *y*, −*z*; #8: *x* − 1/2, 3/2 − *y*, *z* − 1/2, #9: 1 − *x*, 2 − *y*, −*z*, #10: *x* − 1, *y*, *z*.
Centroid codes: *Cg1:* N1, C1, C2, C3, C4, C12; *Cg2:* N2, C10, C9, C8, C7, C11; *Cg3:* N3, C13, C14, C15, C16, C24; *Cg4:* N4, C22, C21, C20, C19, C23; *Cg5:* C4, C5, C6, C7, C11, C12; *Cg6:* C16, C17, C18, C19, C23, C24; *Cg7:* N5, C25, C26, C27, C28, C36; *Cg8:* C35, C36, C28, C29, C30, C31; *Cg9:* N7, C37, C38, C39, C40, C48; *Cg10:* C40, C41, C42, C43, C47, C48; *Cg11*: C43, C44, C45, C46, C47, N8.

A search in Cambridge Structural Database (CSD) [18] shows that five different ways of coordination to two metal centres have been reported for the cyclic anion $\{V_4O_{12}\}^{4-}$, which are summarized in Scheme 1. By most the preferred mode is the bis-chelating mode to two transition metal cations, either with the metals attached to alternate vanadium tetrahedra (type **c**, 17% of the reported cases) or to adjacent ones (type **d**, 61% of the reported cases).

In the present study compounds **1**–**3** show type **d** chelating mode, while compounds **4** and **5** show the rarest coordinating mode of the $\{V_4O_{12}\}^{4-}$ anion: type **e**. To the best of our knowledge only a nickel complex, $[Ni(quaterpy)(H_2O)]^{2+}$, has been reported presenting the vanadium tetranuclear cluster attached to each heterometallic centre through only one bridging oxygen atom [27].

In the case of $[Mn_2(phen)_4V_4O_{12}]\cdot 0.5H_2O$ [28] and $[Co_2(phen)_4V_4O_{12}]\cdot H_2O$ [29,30], the molecular units appear very similar to the ones herein informed, both in geometry and in coordination modes. It is perhaps worth noting that solvatomorphs of structure **2** have already been reported [29,30], but crystallizing in different crystal systems due to the different solvent content (Table 6). Interestingly, the chelating mode reported by Lu et al. [30] (type **c**) is markedly different to the one herein presented (type **d**). The mentioned examples permit to conclude that is quite common for a single constituent to exist in more than one crystalline arrangement [31].

In our system the metal centre is coordinated to two phenanthroline groups in *cis* positions. The octahedral coordination of manganese(II), cobalt(II) and nickel(II) is more favourable to the chelating mode of the cyclovanadate, while the square planar pyramidal environment of the copper (II) ions precludes the chelating mode, and leads to a monodentate mode. In the case of the reported $[Ni(quaterpy)(H_2O)]^{2+}$ complex [27], a geometrical consideration has to be taken into account to explain the monodentate mode: the four nitrogen atoms of the planar ligand form the basal plane around the nickel centre. Only the apical positions can be used to connect the nickel ion to the $\{V_4O_{12}\}^{4-}$ entities. Steric constraints of the 2,2′,6′,2″,6″,2‴-quaterpyridine ligand rule out the possibility of the chelating mode of the cyclovanadate.

3.2. Magnetic properties

The variation in the molar magnetic susceptibilities of complexes **1**–**5** was recorded at 0.1 T, in the temperature range of 2–300 K and is shown as $\chi_M T$ vs T plots in Fig. 4. Solvatomorphs **4** and **5** show the same magnetic behaviour, and only the data corresponding to **4** will be analyzed. The overall magnetic behaviour of the studied complexes can be attributed to very weak antiferromagnetically coupled systems.

For complex **1**, the $\chi_M T$ at 300 K is 5.87 $cm^3\ mol^{-1}$ K which is greater than the expected value of 3.75 $cm^3\ mol^{-1}$ K expected for two uncoupled $S = 3/2$ centres (spin-only $g = 2.00$). However, Co^{II} ions often exhibit large g values around 2.50 due to spin orbit effect. The $\chi_M T$ values decrease gradually to the value of 3.06 $cm^3\ mol^{-1}$ K at low temperature.

The $\chi_M T$ values at 300 K are 9.09 $cm^3\ mol^{-1}$ K for **2**, 2.50 $cm^3\ mol^{-1}$ K for **3** and 0.83 $cm^3\ mol^{-1}$ K for **4** which are as expected for two uncoupled M^{II} = Mn, Ni or Cu ions with reasonable values of g around 2.04 for **2**, 2.23 for **3** or 2.10 for **4**. With decreasing temperature, the $\chi_M T$ values remain almost constant until ca. 29 K for compound **2**, 17 K for compound **3** and 10 K for compound **4**, and then decrease, giving minimum values of 6.70 $cm^3\ mol^{-1}$ K for **2**, 1.66 $cm^3\ mol^{-1}$ K for compound **3** and 0.80 $cm^3\ mol^{-1}$ K for compound **4** at 2 K. A different thermal dependence of the magnetic behaviour was reported by Gu et al. for a solvatomorph of $[Mn_2(bipy)_4V_4O_{12}]$ [32]. They observed that upon cooling the obtained $\chi_M T$ product decreased for the Mn^{II} compound, and it attained a minimum value near 46 K. Below this temperature $\chi_M T$ increased abruptly to reach a maximum between 46 and 39 K, and in the very low temperature range it again started to decrease. Since the structure of this compound was shown by us to remain unaltered at low temperatures, the reported magnetic behaviour, which is different from that observed by us for **2**, can be explained by assuming the presence of ferromagnetic impurities, due to the formation of nanoparticles of manganese (II) oxide during the solvothermal synthesis [33].

As indicated in Section 3.1, the structures of **1**–**4** consist of cobalt, manganese, nickel or copper entities linked between them by a $\{V_4O_{12}\}^{4-}$ anion, giving a dinuclear system. The structure of the manganese containing compound was checked at different temperatures (300 K, 120 K and 30 K). The result was that no structural changes were observed that could affect the magnetic properties. Thus, only one coupling parameter (J) was considered in all the cases to interpret a possible magnetic interaction in the complex.

Taking into account these considerations, with the exception of the cobalt dinuclear compound, in which the presence of spin-orbit coupling effect makes the interpretation of magnetic data more complex, the experimental magnetic data have been fitted using the Eqs. (1)–(3) which are derived from the isotropic Heisenberg Hamiltonian $\mathscr{H} = -JS_1S_2$, considering, $S_{Mn(II)} = 5/2$, $S_{Ni(II)} = 1$, and

$S_{Cu(II)} = 1/2$, respectively, and assuming that the two paramagnetic metal ions have the same g value [34].

The results of the fits are illustrated in Fig. 4, with a smooth curve representing the theoretical calculation. The calculated curves

$$\chi_M = \frac{Ng^2\beta^2}{kT}\frac{2\exp(x) + 10\exp(3x) + 28\exp(6x) + 60\exp(10x) + 110\exp(15x)}{1 + 3\exp(x) + 5\exp(3x) + 7\exp(6x) + 9\exp(10x) + 11\exp(15x)} \quad (1)$$

$$\chi_M = \frac{Ng^2\beta^2}{kT}\frac{2\exp(x) + 10\exp(3x)}{1 + 3\exp(x) + 5\exp(3x)} \quad (2)$$

$$\chi_M = \frac{Ng^2\beta^2}{kT}\frac{2\exp(x)}{1 + 3\exp(x)} \quad (3)$$

$$x = J/kT$$

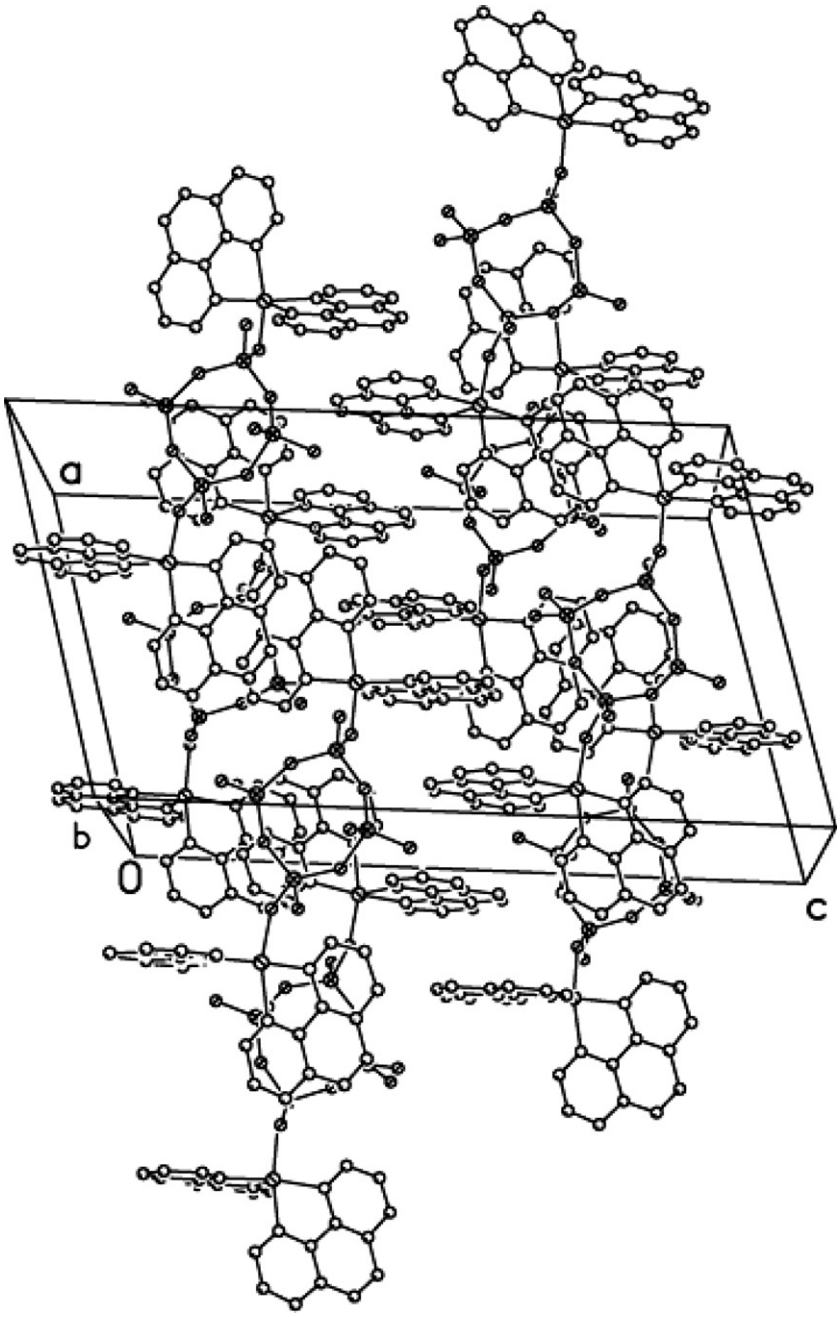

Fig. 3. Packing view of **5**. Hydrogen atoms and disorder on the V_4O_{12} cyclic anion have been omitted for clarity.

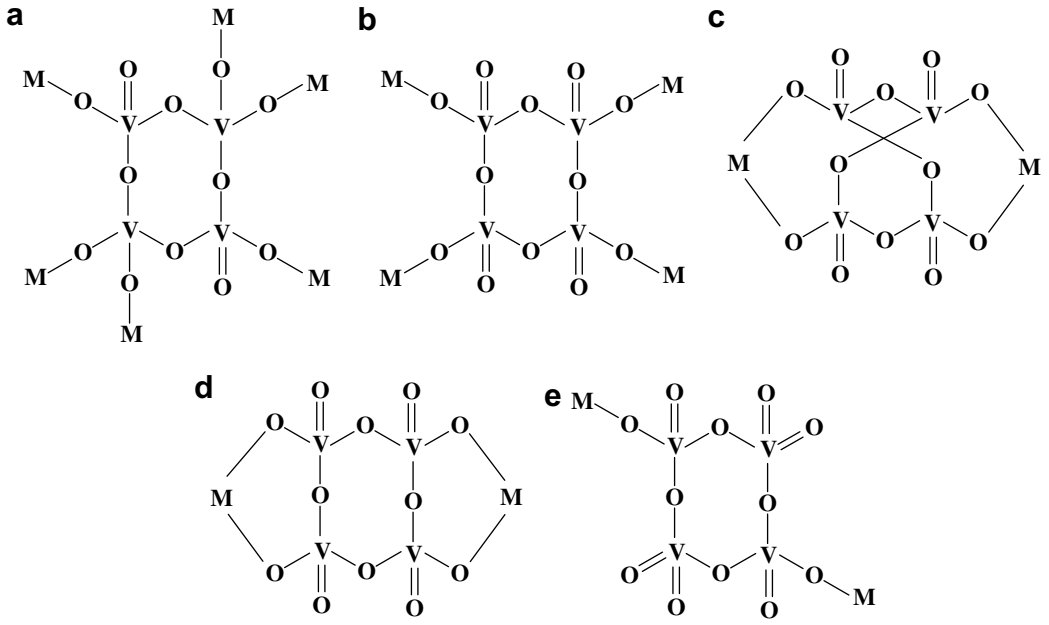

Scheme 1. Different coordination modes of the cyclic anion $\{V_4O_{12}\}^{4-}$.

Table 6
Crystalline parameters of $[M_2(phen)_4V_4O_{12}] \cdot n$ solvent, solvatomorphs

Compound	Ref. [28]	Ref. [29]	Ref. [30]	(**1**)	(**2**)	(**3**)
Formulae	$Mn_2C_{48}H_{32}N_8V_4O_{12} \cdot 0.5H_2O$	$Co_2C_{48}H_{32}N_8V_4O_{12} \cdot H_2O$	$Co_2C_{48}H_{32}N_8V_4O_{12}$	$Co_2C_{48}H_{32}N_8V_4O_{12} \cdot C_6H_{11}OH \cdot H_2O$	$Mn_2C_{48}H_{32}N_8V_4O_{12} \cdot C_6H_{11}OH \cdot H_2O$	$Ni_2C_{48}H_{32}N_8V_4O_{12} \cdot C_6H_{11}OH \cdot H_2O$
Crystal system	Monoclinic	Monoclinic	Orthorhombic	Triclinic	Triclinic	Triclinic
Space group	*P*21/*c*	*P*21/*c*	*Pbcn*	$P\bar{1}$	$P\bar{1}$	$P\bar{1}$
a (Å)	18.47	18.22	19.16	10.6488(15)	10.6860(14)	10.5882(18)
b (Å)	11.47	11.31	15.19	10.6658(15)	10.6781(14)	10.6683(18)
c (Å)	23.66	23.47	16.31	13.0837(18)	13.0960(18)	13.0670(2)
α (°)	90.00	90.00	90.00	75.678(2)	76.732(2)	75.320(3)
β (°)	97.76	97.8	90.00	89.060(2)	89.394(2)	88.914(3)
γ (°)	90.00	90.00	90.00	68.608(2)	69.180(2)	68.434(3)

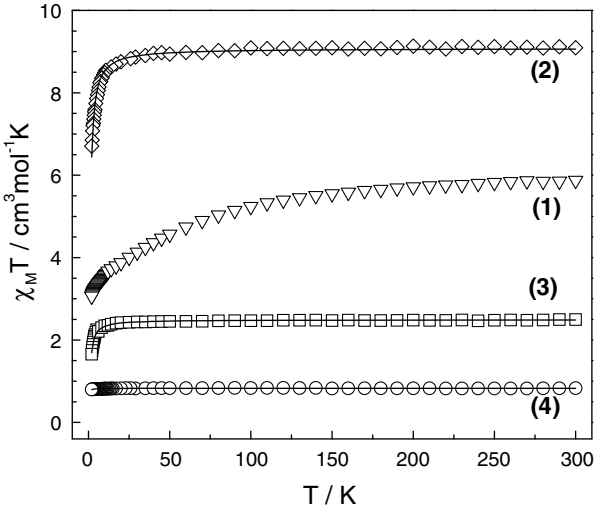

Fig. 4. Plots of $\chi_M T$ vs T for the $[M_2(phen)_4V_4O_{12}] \cdot C_6H_{11}OH \cdot H_2O$ complexes (**1**–**4**). Solid lines represent the best theoretical fit of the experimental data (see text).

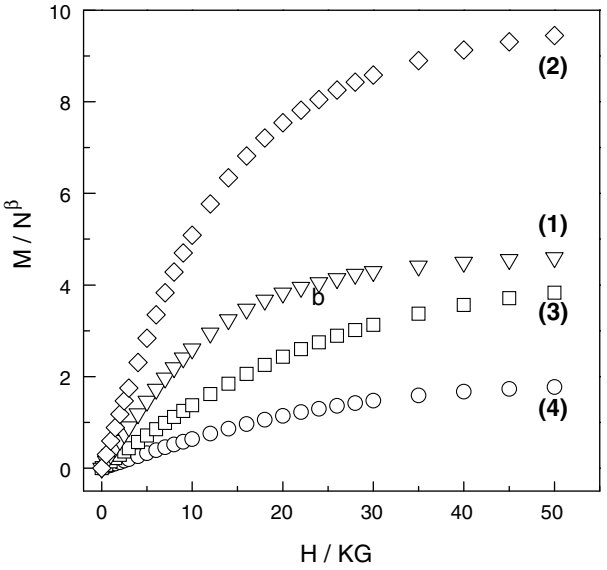

Fig. 5. The field dependence of magnetization at 2 K for $[M_2(phen)_4V_4O_{12}] \cdot C_6H_{11}OH \cdot H_2O$ complexes (**1**–**4**).

match well with the experimental data in all the temperature ranges. The best fit parameters from 300 down to 2 K are found to be: $J = -0.14\ cm^{-1}$ and $g = 2.04$ for compound **2**, $J = -0.64\ cm^{-1}$ and $g = 2.23$ for compound **3**, and $J = -0.23\ cm^{-1}$ and $g = 2.10$ for compound **4**. In all the calculations the agreement factor $R = \sum[(\chi_M T)_{exp} - (\chi_M T)_{calc}]^2/\sum[(\chi_M T)_{exp}]^2$ was lower than 2.7×10^{-6}. It is necessary to indicate that we have not considered the slight differences observed in the crystallographic data among the two molecules **A** and **B** that form compound **4**, and we have considered only one value for the J and g parameters for both molecules **A** and **B**.

From the obtained J values it is possible to conclude that the antiferromagnetic coupling is weakly transmitted through the vanadate bridge, bonding the metal ions in a bi- or monodentate way as in compounds **1**–**5**; this is due to the large M–M distances found in the studied complexes.

The field dependence of the reduced magnetization ($M/N\beta$) (0–5 T) vs H measured at 2 K for the four complexes is shown in Fig. 5. At 5 T, $M/N\beta$ tends to 9.4, 3.8 and 1.8 electrons for compounds **2**–**4**, respectively, which are close to the expected $S = 5/2$ for the two uncoupled Mn^{II} ions, $S = 2$ for the two uncoupled Ni^{II} ions, $S = 1/2$ for the two uncoupled Cu^{II} ions, respectively. The small deviation observed can be attributed to the presence of the low antiferromagnetic behaviour manifested by compounds **2**–**5**. For complex **1**, $M/N\beta$ tends to 3.5 electrons, which is a low value compared to the expected one for $S = 3/2$ for two Co^{II} ions. In this case it is necessary to consider first, the spin orbit effect that characterizes the cobalt(II) ion in an octahedral environment, which results in an effective spin of 1/2 for cobalt atom with a high g value [35,36], and second, the possible presence of a small antiferromagnetic interaction between the cobalt centres in the dimer, as was observed for complexes **2**–**5.**

4. Conclusions

The hydrothermal syntheses overcome the limitation of being able to synthesize only the thermodynamic dense phases, obtained by ceramic methods, and provide a route for the design of inorganic/organic hybrid materials. The use of different solvent media to obtain polymetallic compounds has been shown to lead to similar molecular structures, but different solvatomorphs which crystallize in different symmetries. The studied solvatomorph systems presented similar magnetic properties.

The coordination preferences of the divalent cations of the metals of the first transition row are reflected in the structures of this study. The tendency of Co^{II}, Mn^{II} and Ni^{II} to exhibit six coordination modes is evident in the structures of **1**, **2** and **3**. In contrast, the plasticity of Cu^{II} became evident with the pentacoordination of the metal centre in $[Cu_2(phen)_4V_4O_{12}]$. This is the first example of a discrete copper(II) dinuclear complex with a monodentate bridging cyclovanadate.

In the present work the oxidation of V^{IV} is observed and permits the isolation of $[Cu_2(phen)_4V_4O_{12}]$ from the V_2O_4 precursor. This oxidation reaction can be ascribed to the presence of $Cu(NO_3)_2$ in the reacting medium.

The magnetic study carried out on compounds **1**–**5** indicated a very low intramolecular magnetic exchange interaction between the paramagnetic Co^{II}, Mn^{II}, Ni^{II} and Cu^{II} centres through the –O–V–O–V–O– bridge, due to the large M–M distances, that range from 7.87 to 10.97 Å.

Acknowledgments

The authors acknowledge FONDAP 11980002, DVY and ES FONDECYT 1080316 projects for financial support. M.S. thanks CONICYT for a doctoral scholarship. Spanish Grants extended by the Ministerio de Educación y Ciencia (CTQ2006-01759) are also gratefully acknowledged. We thank A. Goeta (Durham University, UK) for the recording of diffraction data at low temperature.

Appendix A. Supplementary material

Supplementary data associated with this article can be found, in the online version, at doi:10.1016/j.ica.2008.03.098.

References

[1] S. Aswanden, H.W. Schamalle, A. Reller, H.R. Oswald, Mater. Res. Bull. 28 (1993) 45.
[2] R. Nandini, J. Zubieta, Inorg. Chim. Acta 343 (2003) 313.
[3] J.Y. Xie, J.G. Mao, J. Mol. Struct. 750 (2005) 186.
[4] R. Nandini, J. Zubieta, Inorg. Chim. Acta 338 (2002) 165.
[5] Y. Zhang, P.J. Zapf, L.M. Meyer, R.C. Haushalter, J. Zubieta, Inorg. Chem. 36 (1997) 2159.
[6] V.W. Day, W.G. Klemperer, A. Yagasaki, Chem. Lett. (1990) 1267.
[7] G.Y. Yang, D.W. Gao, Y. Chen, J.Q. Xu, Q.X. Zeng, H.R. Sun, Z.W. Pei, Q. Su, Y. Xing, H.Q. Ling, Acta Crystallogr., Sect. C 54 (1998) 6161.
[8] H. Akashi, K. Isobe, Y. Ozawa, A.J. Yagasaki, Cluster Sci. 2 (1991) 291.
[9] Y. Hayashi, Y. Ozawa, K. Isobe, Chem. Lett. (1989) 425.
[10] C.M. Liu, S. Gao, H.M. Hu, Z.M. Wang, Chem. Commun. (2001) 1636.
[11] X.M. Zhang, M.L. Tong, X.M. Chen, Chem. Commun. (2000) 1817.
[12] Y. Qi, Y. Wang, H. Li, M. Cao, Ch Hu, E. Wang, N. Hu, H. Jia, J. Mol. Struct. 650 (2003) 123.
[13] L.C.W. Baker, D.C. Glick, Chem. Rev. 98 (1998) 3.
[14] B.E. Koene, N.J. Taylor, L.F. Nazar, Angew. Chem., Int. Ed. Engl. 38 (1999) 2888.
[15] G. Senti, F. Trifiro, Appl. Catal. A. 143 (1996) 3.
[16] M.I. Khan, E. Yohannes, R.C. Nome, S. Ayesh, V.O. Golub, C.J. O'Connor, R.J. Doedens, Chem. Mater. 16 (2004) 5273.
[17] M.I. Khan, S. Deb, R.J. Doedens, Inorg. Chem. Commun. 9 (2006) 25.
[18] The Cambridge Structural Database: a quarter of a million crystal structures and rising F.H. Allen, Acta Crystallogr., Sect. B 58 (2002) 380.
[19] SMART NT V5.625 Bruker AXS Inc., Madison, WI, USA.
[20] RLATT V3.0 Bruker AXS Inc., Madison, WI, USA.
[21] SAINTPLUS V6.22 Bruker AXS Inc., Madison, WI, USA.
[22] G.M. Sheldrick, SHELXTL NT/2000 Version 6.10., Bruker AXS Inc., Madison, WI, USA, 2000.
[23] SADABS V2.05 Bruker AXS Inc., Madison, WI, USA.
[24] P. Roman, A. Aranzabe, A. Luque, J.M. Gutierrez-Zorrilla, Mater. Res. Bull. 26 (1991) 19.
[25] S. Ushak, E. Spodine, D. Venegas-Yazigi, E. Le Fur, J.Y. Pivan, O. Peña, R. Cardoso-Gil, R. Kniep, J. Mater. Chem. 15 (2005) 4529.
[26] W. Ouellette, M.H. Yu, J. O'Connor, J. Zubieta, Inorg. Chem. 45 (2006) 3224.
[27] D. Xiao, Y. Hou, E. Wang, J. Lu, Y. Li, L. Xu, Ch Hu, Inorg. Chem. Commun. 7 (2004) 437.
[28] Y. Lu, E. Wang, M. Yuan, Y. Li, L. Xu, Ch Hu, N. Hu, H. Jia, Solid State Sci. 4 (2002) 449.
[29] R. Kucsera, R. Gyepes, L. Zurkova, Cryst. Res. Technol. 37 (2002) 890.
[30] Y. Lu, E.B. Wang, M. Yuan, Y.G. Li, C.W. Hu, N.H. Hu, H.Q. Jia, J. Mol. Struct. 607 (2002) 189.
[31] G.P. Stahly, Cryst. Growth Des. 7 (2007) 1007.
[32] W. Gu, H.D. Bian, J.Y. Xu, S.P. Yan, D.Z. Liao, Z.H. Jiang, Inorg. Chem. Commun. 6 (2003) 217.
[33] G.H. Lee, S.H. Huh, J.W. Jeong, B.J. Choi, S.H. Kim, Y.Z. Ri, J. Am. Chem. Soc. 124 (2002) 12094.
[34] C.J. O'Connor, Prog. Inorg. Chem. 29 (1982) 203.
[35] O. Kahn, Molecular Magnetism, Wiley-VCH Inc., USA, 1993.
[36] B.P. Yang, A.V. Prosvirin, Y.Q. Guo, J.G. Mao, Inorg. Chem. 47 (2008) 1453.